J. Fluid Mech. (1975), *vol.* 70, *part* 4, *pp.* 689–703
Printed in Great Britain

Numerical simulation of two-dimensional compressible convection

By ERIC GRAHAM

Department of Applied Mathematics and Theoretical Physics,
University of Cambridge

(Received 27 June 1974 and in revised form 1 February 1975)

A procedure for obtaining numerical solutions to the equations describing thermal convection in a compressible fluid is outlined. The method is applied to the case of a perfect gas with constant viscosity and thermal conductivity. The fluid is considered to be confined in a rectangular region by fixed slippery boundaries and motions are restricted to two dimensions. The upper and lower boundaries are maintained at fixed temperatures and the side boundaries are thermally insulating. The resulting convection problem can be characterized by six dimensionless parameters. The onset of convection has been studied both by obtaining solutions to the nonlinear equations in the neighbourhood of the critical Rayleigh number R_c and by solving the linear stability problem. Solutions have been obtained for values of the Rayleigh number up to $100R_c$ and for pressure variations of a factor of 300 within the fluid. In some cases the fluid velocity is comparable to the local sound speed. The Nusselt number increases with decreasing Prandtl number for moderate values of the depth parameter. Steady finite amplitude solutions have been found in all the cases considered. As the horizontal dimension A of the rectangle is increased, the length of time needed to reach a steady state also increases. For large values of A the solution consists of a number of rolls. Even for small values of A, no solutions have been found where one roll is vertically above another.

1. Introduction

Most work on convection is based upon the Boussinesq approximation, which is valid for a compressible fluid only when both the vertical density variation and the motion-induced fluctuations are small (Spiegel & Veronis 1960). In the areas of astrophysics and meteorology, convection can extend over one or more pressure scale heights and the use of the Boussinesq approximation may lead to gross errors.

The anelastic approximation (Ogura & Phillips 1962; Gough 1969) removes the restriction on the total density variation while still requiring that the relative density fluctuations produced by the motion be small. As we shall see later, quite moderate values of the parameters describing convection can lead to such vigorous motion that this restriction is violated.

It seems worthwhile, therefore, to seek finite amplitude solutions of the full

equations without making any assumptions about the magnitudes of the velocity and density variations.

This paper describes a numerical procedure for solving the full equations of motion of a compressible viscous fluid with heat conduction. For reasons of computational expediency, the method is applied to strictly two-dimensional motion. The solutions of small amplitude are compared with numerical solutions of the equations of the linear stability problem. Large amplitude solutions are calculated to show how such properties as the heat flux and convective velocity depend upon the boundary conditions.

The aim of this work is to establish a procedure for generating standard solutions so that other, more approximate, methods for treating convection (see, for example, Spiegel 1971, 1972) can be tested for a much wider range of parameters than would be possible if laboratory results alone were available. In particular, these results can provide a test for the truncated modal expansion techniques which have been applied by Gough, Spiegel & Toomre (1969, private communication) to the Boussinesq case and by Latour (1972) and Latour *et al.* (1974) to the anelastic case.

2. The equations and parameters of the problem

The equations of motion for a compressible viscous gas with heat conduction are

$$\partial\rho/\partial t + \partial(\rho u_i)/\partial x_i = 0, \tag{2.1}$$

$$\rho\left(\frac{\partial u_i}{\partial t} + u_j\frac{\partial u_i}{\partial x_j}\right) + \frac{\partial p}{\partial x_i} - \frac{\partial \tau_{ij}}{\partial x_j} - g_i\rho = 0 \tag{2.2}$$

and

$$\rho T\left(\frac{\partial S}{\partial t} + u_i\frac{\partial S}{\partial x_i}\right) - \tau_{ij}\frac{\partial u_i}{\partial x_j} - \frac{\partial}{\partial x_i}K\frac{\partial T}{\partial x_i} = 0, \tag{2.3}$$

where

$$\tau_{ij} = \eta\left(\frac{\partial u_i}{\partial x_j} + \frac{\partial u_j}{\partial x_i} - \tfrac{2}{3}\delta_{ij}\frac{\partial u_l}{\partial x_l}\right) + \delta_{ij}\eta_1\frac{\partial u_l}{\partial x_l}. \tag{2.4}$$

S is the specific entropy, η and η_1 are the coefficients of viscosity and K is the conductivity. All the other symbols have their usual meaning and summation over repeated subscripts is implied.

After some manipulation, (2.2) and (2.3) can be rearranged into conservation-law form:

$$\frac{\partial}{\partial t}(\rho u_i) + \frac{\partial}{\partial x_j}(\delta_{ij}p + \rho u_i u_j - \tau_{ij}) - g_i\rho = 0, \tag{2.5}$$

$$\frac{\partial}{\partial t}[\rho(\tfrac{1}{2}u_j u_j + E + \phi)] + \frac{\partial}{\partial x_i}[\rho u_i(W + \tfrac{1}{2}u_j u_j + \phi) - K(\partial T/\partial x_i) - u_j\tau_{ij}] = 0, \tag{2.6}$$

where

$$\phi = gx_2, \quad g_i = -g\delta_{i2}. \tag{2.7}$$

E is the internal energy and W is the enthalpy of the gas. The second co-ordinate axis is taken to be vertical.

For simplicity we shall assume that the gas obeys a perfect-gas law and that the specific heats, the coefficients of viscosity and the conductivity are all constant. Thus

$$p = R_* \rho T, \tag{2.8}$$

$$c_v = \alpha R_*, \quad c_p = (1+\alpha) R_*, \tag{2.9), (2.10}$$

$$W = c_p T, \quad E = c_v T, \tag{2.11), (2.12}$$

$$\gamma = c_p/c_v = (1+\alpha)/\alpha \tag{2.13}$$

and

$$S = R_*(\alpha \log T - \log \rho). \tag{2.14}$$

2.1. *Boundary conditions*

We suppose that motion is two-dimensional with no velocity or temperature gradients in the x_3 direction. The least restrictive conditions to apply at the walls are free boundary conditions. The upper and lower walls are maintained at prescribed temperatures and the side walls are thermally insulating. The boundary conditions are

$$u_2 = \partial u_1/\partial x_2 = 0, \quad T = T_l, T_u \quad \text{at} \quad x_2 = 0, a_2 \tag{2.15}$$

and

$$u_1 = \partial u_2/\partial x_1 = \partial T/\partial x_1 = 0 \quad \text{at} \quad x_1 = 0, a_1. \tag{2.16}$$

2.2. *Static state*

A solution of the equations is given by the hydrostatic and thermal equilibrium equations with $u_1 = u_2 = 0$. Following Spiegel (1965) we can show that

$$T_0 = \beta_0 z, \quad \rho_0 = (C/R_* \beta_0) z^m, \quad p_0 = C z^{m+1}, \tag{2.17)–(2.19}$$

where

$$\beta_0 = \frac{T_l - T_u}{a_2}, \quad m = \frac{g}{R_* \beta_0} - 1, \quad z = \frac{T_u}{\beta_0} + a_2 - x_2. \tag{2.20)–(2.22}$$

m is the polytropic index and C is an integration constant, its value depending upon the mass contained within the boundaries.

The entropy gradient can be calculated as

$$dS/dx_2 = g(m-\alpha)/(m+1). \tag{2.23}$$

In our case this is a constant. If we consider an adiabatic displacement of a small parcel of gas maintained in pressure equilibrium with its surroundings, buoyancy forces will act to return the parcel to its original location if the local entropy gradient is positive. A necessary condition for the onset of convection is that the local entropy gradient be negative. In the astrophysical literature this is known as the Schwarzschild criterion.

If we subject the static state to a small perturbation and use this to provide initial conditions, our convection problem is specified by the ten parameters R_*, the gas constant; γ, the ratio of specific heats; K, the thermal conductivity; η, the dynamic viscosity (we assume that the bulk viscosity η_1 is zero); T_u and T_l, the upper and lower boundary temperatures; a_1 and a_2, the horizontal and vertical cell sizes; g, the gravitational acceleration; and C, which is a measure of the mass of the gas.

Since we are free to choose our units of mass, length, time and temperature, we have six degrees of freedom in setting up a convection experiment. We choose our units such that η, a_2, T_u and the density at the upper boundary for the static solution are all unity. We define an aspect ratio A, a Prandtl number σ, a normalized layer thickness parameter Z, an upper-boundary Rayleigh number R and a horizontal wavenumber a by

$$A = a_1/a_2, \quad \sigma = c_p\eta/K, \quad Z = (T_l - T_u)/T_u \tag{2.24)–(2.26}$$

and

$$R = \frac{(g/T_u)\,a_2^4[(T_l - T_u)/a_2 - g/c_p]}{(K/\rho_u c_p)\,(\eta/\rho_u)}. \tag{2.27}$$

If n is the number of convective rolls in the cell

$$a = n\pi/A. \tag{2.28}$$

The convection experiment can be characterized by the six parameters γ, A, σ, Z, m and R. We note that our definition of Z, m and R is the same as that of Spiegel (1965).

3. The finite-difference scheme

A finite-difference scheme to solve (2.1), (2.5) and (2.6) has been developed. It is a modification of the two-step Lax–Wendroff scheme (see, for example, Richtmyer & Morton 1967, p. 302).

In order to describe this scheme economically, we must introduce some special notation. Let $P(i,j)$ and $Q(i,j)$ represent values of the variables P and Q at a grid point (i,j). The grid spacing δ is the same in both co-ordinate directions. We define averaging and difference operators by

$$\langle P(i,j)\rangle = \tfrac{1}{4}(P(i+1,j)+P(i-1,j)+P(i,j+1)+P(i,j-1)), \tag{3.1}$$

$$\langle P(i,j)\rangle_r = \tfrac{1}{2}(P(i+\tfrac{1}{2},j+\tfrac{1}{2})+P(i-\tfrac{1}{2},j-\tfrac{1}{2})), \tag{3.2}$$

$$\langle P(i,j)\rangle_l = \tfrac{1}{2}(P(i-\tfrac{1}{2},j+\tfrac{1}{2})+P(i+\tfrac{1}{2},j-\tfrac{1}{2})), \tag{3.3}$$

$$\langle P(i,j)\rangle_1 = \tfrac{1}{2}(P(i+1,j)+P(i-1,j)), \tag{3.4}$$

$$\langle P(i,j)\rangle_2 = \tfrac{1}{2}(P(i,j+1)+P(i,j-1)), \tag{3.5}$$

$$\Delta_1 P(i,j) = (P(i+1,j)-P(i-1,j))/2\delta, \tag{3.6}$$

$$\Delta_2 P(i,j) = (P(i,j+1)-P(i,j-1))/2\delta, \tag{3.7}$$

$$\Delta_r P(i,j) = (P(i+\tfrac{1}{2},j+\tfrac{1}{2})-P(i-\tfrac{1}{2},j-\tfrac{1}{2}))/2^{\frac{1}{2}}\delta, \tag{3.8}$$

$$\Delta_l P(i,j) = (P(i-\tfrac{1}{2},j+\tfrac{1}{2})-P(i+\tfrac{1}{2},j-\tfrac{1}{2}))/2^{\frac{1}{2}}\delta, \tag{3.9}$$

$$D_1 P = \langle \Delta_1 P\rangle_2, \quad D_2 P = \langle \Delta_2 P\rangle_1, \tag{3.10), (3.11}$$

$$\Delta_1(P,Q) = \langle P\rangle_1 \Delta_1(Q), \quad \Delta_2(P,Q) = \langle P\rangle_2 \Delta_2(Q), \tag{3.12), (3.13}$$

$$\nabla(P,Q) = \Delta_r(\langle P\rangle_l \Delta_l Q) + \Delta_l(\langle P\rangle_r \Delta_r Q). \tag{3.14}$$

The two-step Lax–Wendroff scheme for an equation of the form

$$\partial U/\partial t + \partial A_m(U)/\partial x_m = 0 \tag{3.15}$$

is

$$U^* = \langle U\rangle - \tau\Delta_m A_m(U), \quad U^{**} = U - 2\tau\Delta_m A_m(U^*), \tag{3.16), (3.17}$$

where τ is the time step. U is the variable evaluated at time t_0. U^* and U^{**} are variable values at time $t_0+\tau$ and $t_0+2\tau$. U^* has only first-order accuracy and is regarded as a provisional value. U^{**} has second-order accuracy. If we consider the value of U at a grid point (i,j) at time $t_0+k\tau$ the difference scheme is seen to give no coupling between the set of points having even values of $i+j+k$ and those having odd values. Half the grid points may be omitted.

If we subtract the hydrostatic equation from the momentum equation (2.5) and perform some manipulations on (2.4)–(2.6) we have

$$\partial\rho'/\partial t+\partial(\rho u_i)/\partial x_i=0, \tag{3.18}$$

$$\frac{\partial}{\partial t}(\rho u_i)+\frac{\partial}{\partial x_j}\left(\delta_{ij}p'+\rho u_i u_j-\eta\frac{\partial u_j}{\partial x_i}+(\tfrac{2}{3}\eta-\eta_1)\,\delta_{ij}\frac{\partial u_l}{\partial x_l}\right)-\frac{\partial}{\partial x_j}\eta\frac{\partial u_i}{\partial x_j}-g_i\rho'=0, \tag{3.19}$$

$$\frac{\partial}{\partial t}[\rho(\tfrac{1}{2}u_j u_j+E+\phi)]'+\frac{\partial}{\partial x_i}\left[\rho u_i(W+\tfrac{1}{2}u_j u_j+\phi)-\eta u_j\left(\frac{\partial u_i}{\partial x_j}+\frac{\partial u_j}{\partial x_i}\right)+(\tfrac{2}{3}\eta-\eta_1)\,u_i\frac{\partial u_l}{\partial x_l}\right]$$
$$-\frac{\partial}{\partial x_i}\left(K\frac{\partial T}{\partial x_i}\right)'=0, \tag{3.20}$$

where a primed quantity represents a fluctuation from the static state. No approximations have been made up to this point. We shall illustrate the difference scheme for the single equation

$$\frac{\partial U}{\partial t}+\frac{\partial}{\partial x_m}\left(A_m(U)+F_n(U)\frac{\partial}{\partial x_n}G_m(U)\right)+\frac{\partial}{\partial x_m}\left(B(U)\frac{\partial}{\partial x_m}C(U)\right)+H(U)=0, \tag{3.21}$$

which contains terms of the same form as can be found in (3.18)–(3.20). The difference scheme is

$$U^*=\langle U\rangle-\tau(\Delta_m(A_m(U)+F_n(U)D_nG_m(U)$$
$$+B(U)D_mC(U))+\langle H(U)\rangle), \tag{3.22}$$

$$U^{**}=U-2\tau(\Delta_m(A_m(U^*)+\Delta_n(F_n(U),G_m(U))$$
$$+\nabla(B(U),C(U))+H(U)). \tag{3.23}$$

These equations are applied to grid points having even values of $i+j+k$. At first it may seem unnecessary to introduce the B and C terms at all since they can readily be expressed in the manner of the F and G terms, as they have been in (3.22). Examination of (3.23) shows that, if B, C and H are zero, then the difference scheme not only conserves the sum of the values of U on all grid points but also separately conserves the sums on the set of points with $i+j+k=4q$ (even–even points) and the set of points with $i+j+k=4q+2$ (even–odd points), where q is an integer. This separate conservation property can lead to the development of a chequer-board instability. The diffusive term $\nabla(B,C)$ serves to couple the even–even and even–odd grids and prevents this instability while still maintaining the overall conservation property. Such diffusive terms are present in the equations for the conservation of momentum and energy while the mass conservation equation does not possess such terms. However, this has not led to any difficulty with the difference scheme.

Because the difference scheme is explicit, we may expect a number of constraints on the time step which must be satisfied if instability is to be avoided. The Courant condition for the two-step Lax–Wendroff scheme requires that

$$\tau < \delta/(|\mathbf{u}| + c)\, 2^{\frac{1}{2}}, \tag{3.24}$$

where c is the adiabatic sound speed. In order to prevent the instability that occurs when explicit difference schemes are applied to simple diffusive equations, we must have

$$\tau < \rho\delta^2 c_p/K \times 2^{\frac{1}{2}}, \quad \tau < \rho\delta^2/\eta. \tag{3.25), (3.26}$$

No formal stability analysis of the difference scheme has been made. The calculations reported here have been made with a time step about half the size of the maximum permitted by (3.24)–(3.26). A grid size of 21×21 has been used for most of the calculations. Experiments with a finer grid seldom differ by more than a few per cent from those using the coarse grid except when the Rayleigh number is so large that sharp boundary layers develop.

4. The onset of convection

A linear stability analysis of the basic equations for a polytrope has been performed by Spiegel (1965). He obtained the equations

$$(D^2 - a^2)\,\theta = \frac{(\beta_0 - g/c_p)\, C c_p d^{m+2}(m+1)\,\zeta^m \omega}{gK} \tag{4.1}$$

and

$$\mathscr{L}(\omega) = -CR_*(m+1)^2 d^{m+1} a^2 \zeta^m \theta/g\eta, \tag{4.2}$$

where

$$\mathscr{L} = \zeta(D^2 - a^2)^2 + \zeta(D^2 - a^2)\, D\frac{m}{\zeta} - (m+1)\,(D^2 - a^2)\left(D + \frac{m}{\zeta}\right) + \frac{m(m+1)}{3\zeta}\, a^2. \tag{4.3}$$

θ is the linearized temperature fluctuation, ω is the vertical velocity, d is the vertical layer thickness, a is the horizontal wavenumber measured in units of d^{-1}, $\zeta = z/d$ and $D = d/d\zeta$. By introducing

$$w = \frac{(\beta_0 - g/c_p)\, C c_p d^{m+2}(m+1)}{gK}\,\omega \tag{4.4}$$

and the definition of the Rayleigh number R, we have

$$(D^2 - a^2)\,\theta = \zeta^m w, \quad \mathscr{L}(w) = RZ^{2m-1} a^2 \zeta^m \theta. \tag{4.5), (4.6}$$

The boundary conditions for free surfaces are

$$w = \theta = D^2 w + (m/\zeta)\, Dw = 0 \quad \text{at} \quad \zeta = Z^{-1}, (1+Z)/Z. \tag{4.7}$$

A variety of numerical methods exists for solving (4.5) and (4.6) for the eigenvalue R. We used a special programming language called BODEL, which we had developed to solve systems of ordinary and partial differential equations. The input to the BODEL compiler is a system of first-order ordinary differential equations. The compiler automatically generates a set of difference equations, which are solved by a generalized Newton–Raphson method. By constructing a series of solutions with varying values of the wavenumber, the minimum Rayleigh number and the corresponding critical wavenumber a_c can be found.

The variation of R_c as a function of a is shown for a number of values of Z in figure 1. Solutions of the linear equations have also been obtained by Vickers

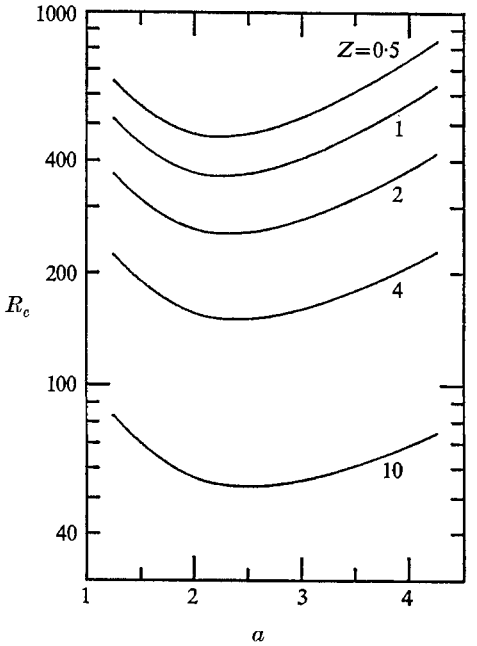

FIGURE 1. Critical Rayleigh number of a polytrope of index 1·4 as a function of wavenumber for different values of the depth parameter.

(1971) and Moore (1973, private communication). Whereas Moore's results are in complete agreement with those of this study, Vickers' values for the Rayleigh number are 50 % larger, while his eigenfunction exhibits a sharp spike near $\zeta = 0$ which we did not find.

We can use the critical Rayleigh number calculated from the solution of the linear equations to test the method for solving the full nonlinear equations. We choose as initial conditions the temperature and density fields of the static solution with a velocity field of small amplitude which satisfies the boundary conditions. After integrating the full equations for a sufficient length of time for transient effects to disappear, an exponentially growing (or decaying) velocity field is found. By repeating the calculation for different values of R it is straightforward to find the value of R for which the growth rate is zero (i.e. the critical Rayleigh number). The difference between the critical Rayleigh numbers calculated from the full equations and the linear equations has never been found to be more than 4 % even when a coarse grid was used.

5. Numerical solutions

The linear problem for the onset of convection is specified by the three parameters Z, a and m. From these we can compute R_c as an eigenvalue. We have seen that the nonlinear problem requires specification of at least six parameters: Z, A, m, γ, σ and R. If, after a sufficient length of time, a steady solution is found, there is no guarantee that this solution is unique. Different initial conditions may result in different steady solutions.

In order to gain some insight into compressible convection, we shall examine how the steady solution changes as we change each of the six parameters. In this survey we define the Nusselt number as

$$N = (F_t - F_a)/(F_c - F_a), \tag{5.1}$$

where F_a is the flux due to the adiabatic gradient,

$$F_a = gK/c_p, \tag{5.2}$$

F_t is the total heat flux and F_c is the conductive heat flux of the static state,

$$F_c = K(T_l - T_u)/a_2. \tag{5.3}$$

This definition of the Nusselt number has been chosen because it coincides, for small layer thickness, with the normal definition used in Boussinesq theory. We shall characterize the velocity of the flow by $\mathscr{M}$, the maximum Mach number.

Instead of dealing directly with the ratio of specific heats, we shall employ the parameter α defined by (2.13), which is the polytropic index of an adiabatic configuration. In many physical situations, the polytropic index is close to the adiabatic value, so it is useful to deal with the super-adiabatic excess $\alpha - m$.

Let us introduce a relative Rayleigh number

$$\lambda = R/R_c, \tag{5.4}$$

where $R_c = R_c(a, Z, m)$ is the critical Rayleigh number calculated from the linear equations.

We choose as the starting point of our survey the values $A = 1$, $\sigma = 1$, $\alpha = 1{\cdot}5$, $m = 1{\cdot}4$ and $Z = 1$ and refer to the solution for these values as the standard solution. The initial conditions are

$$\rho = \rho_0, \quad T = T_0, \tag{5.5), (5.6}$$

$$u_1 = \sum_{i=1}^{N_x} \sum_{j=1}^{N_y} U_{ij} \sin\frac{i\pi x_1}{a_1} \cos\frac{j\pi x_2}{a_2} \frac{a_1}{i\rho_0}, \tag{5.7}$$

$$u_2 = -\sum_{i=1}^{N_x} \sum_{j=1}^{N_y} U_{ij} \cos\frac{i\pi x_1}{a_1} \sin\frac{j\pi x_2}{a_2} \frac{a_2}{j\rho_0}. \tag{5.8}$$

A number of values of N_x, N_y and U_{ij} were tried, but in each case the solution evolved to the same steady state. The time taken to reach a steady state was approximately one viscous time scale.

The horizontal averages of the temperature, density and pressure distributions are shown in figure 2 (*a*). The flow pattern is shown in figure 2 (*b*). The length of each arrow in this figure is proportional to the velocity. The arrows are distributed at random with a probability proportional to the fluid density. We observe that, although the density varies by a factor of 2·6, the velocities along the upper and lower faces are remarkably similar. It might be argued that the velocity in the low density region should be larger in order to satisfy the continuity equation. This is not the case because we adopted a constant dynamic viscosity, so that the kinematic viscosity, and thus the boundary-layer thickness, is larger in the low density region.

Now let us examine the effect of varying each of the six parameters.

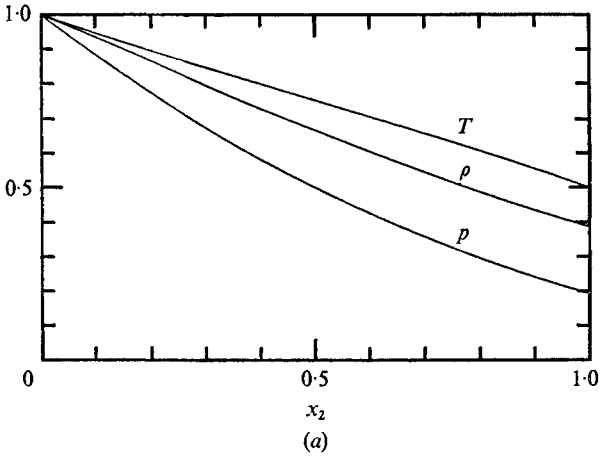

(*a*)

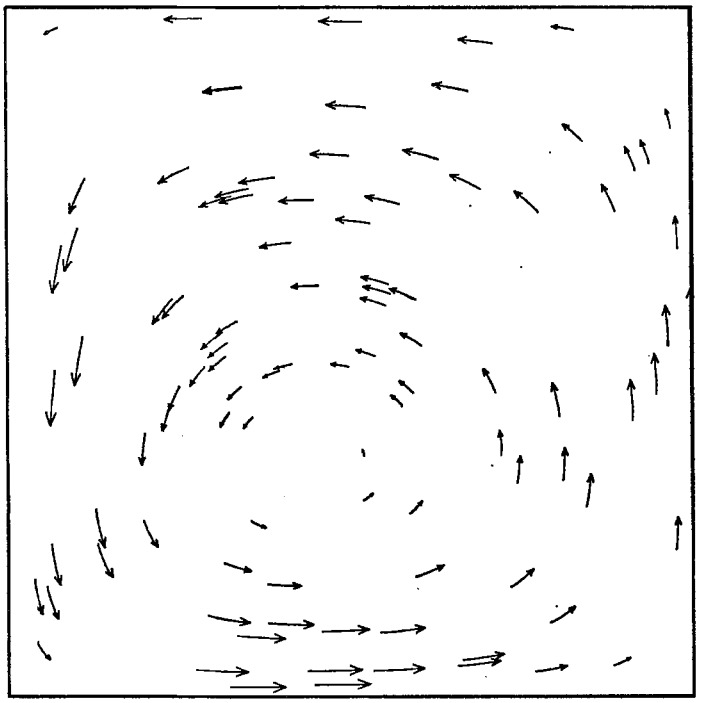

(*b*)

FIGURE 2. The standard solution. (*a*) The mean temperature, density and pressure fields. (*b*) The velocity field. Grid size = 21 × 21. Time = 2.

5.1. *The depth parameter*

The effect of varying Z is shown in figures 3(*a*) and (*b*). All the parameters have their standard values except for Z. We see that, while N decreases slightly with increasing Z, the Mach number increases sharply. It is not feasible to compute solutions with small values of Z (i.e. in the Boussinesq regime) because the maximum time step allowed for numerical stability by (3.24) becomes small,

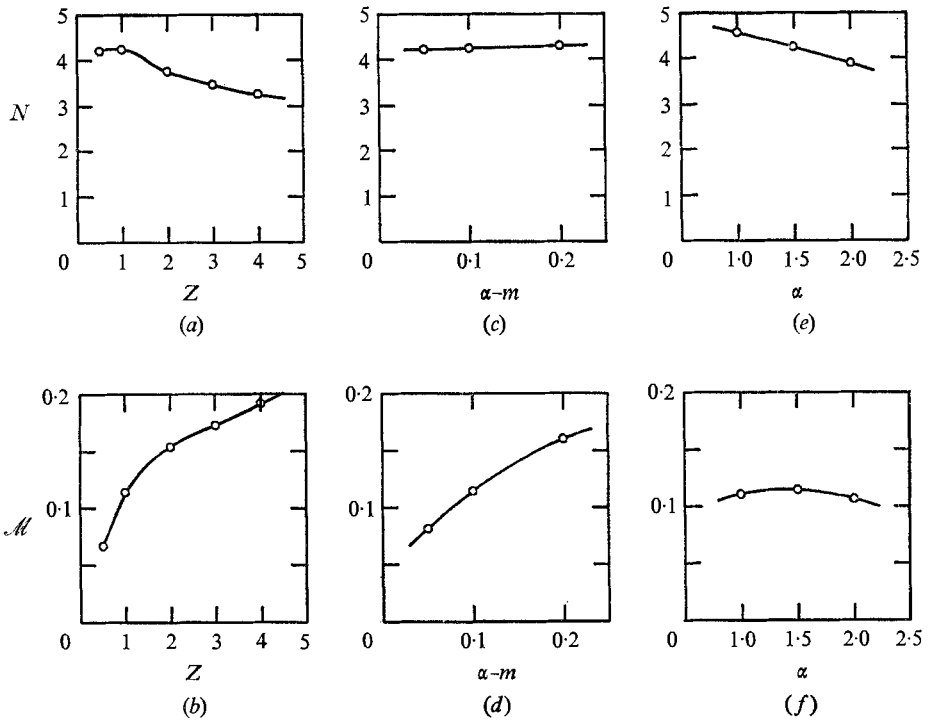

FIGURE 3. Nusselt number and maximum Mach number as functions of Z, $\alpha - m$ and α. The remaining parameters have their standard values. Grid size = 21 × 21.

requiring large amounts of computer time. For large values of Z, errors are introduced in trying to resolve the large density and pressure variations with the finite-difference grid. At $Z = 4$, the pressure varies by a factor of 50 between the upper and lower surfaces.

5.2. *The super-adiabatic excess*

Figures 3 (*c*) and (*d*) show how N and $\mathscr{M}$ depend upon the excess $\alpha - m$. We see that N is quite insensitive to $\alpha - m$. This is due to the way we defined N. The value of F_t/F_c tends to unity as $\alpha - m$ tends to zero. The convective velocity increases rapidly with increasing super-adiabatic excess.

5.3. *The ratio of specific heats*

Figures 3 (*e*) and (*f*) show the result of varying α and m such that $\alpha - m = 0{\cdot}1$. We see that neither N nor $\mathscr{M}$ depends sensitively on α provided that the super-adiabatic excess is kept constant.

5.4. *The Prandtl number*

Figures 4 (*a*) and (*b*) show the variation of N and $\mathscr{M}$ as functions of σ when all the other parameters have their standard values. We notice a large increase in N as σ is reduced below 0·5. For $\sigma = 0{\cdot}1$ the fluid velocity exceeds half the local sound speed. The flow field is still similar to the field for $\sigma = 1$ except that the upper-face

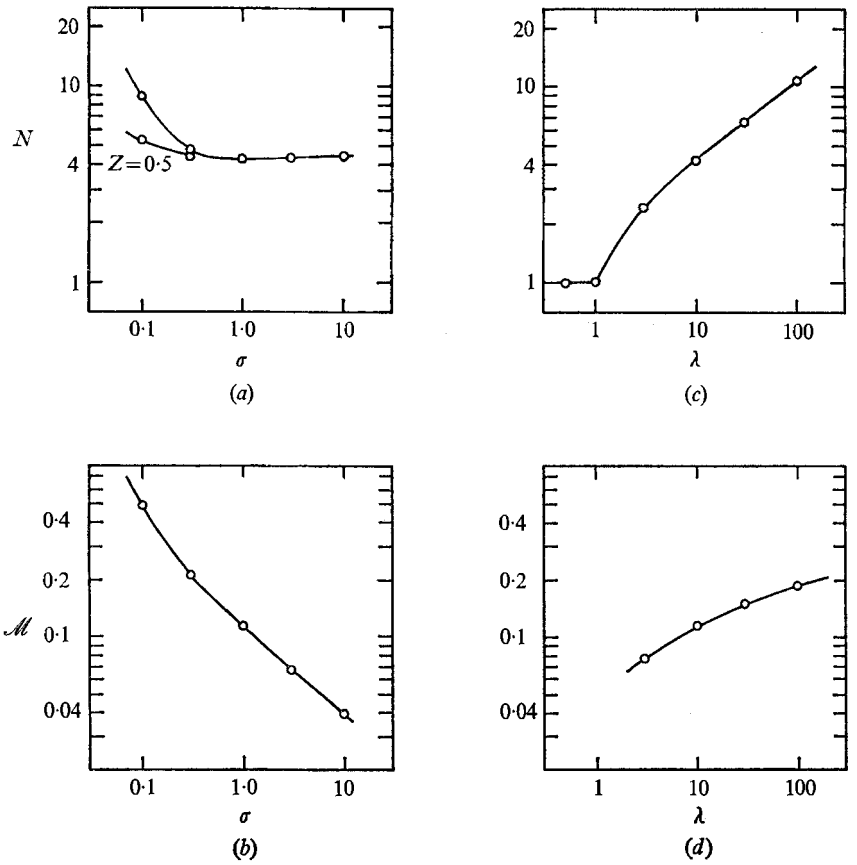

FIGURE 4. Nusselt number and maximum Mach number as functions of Prandtl number and relative Rayleigh number. All other parameters have their standard values except in (*a*), which also shows $Z = 0{\cdot}5$. Grid size = 21×21.

velocity is half the size of the velocity across the lower face. The large velocities give rise to departures of the density distribution from the static-state distribution of up to 40 %. Figure 4 (*a*) also shows the variation of N with σ for $Z = 0{\cdot}5$ instead of $Z = 1$. We see that the enhancement of the Nusselt number at low Prandtl numbers is much reduced for this smaller value of Z. This is to be expected since the results for the Boussinesq approximation, for which Z tends to zero (see, for example, Moore & Weiss 1973), show changes of less than 5 % in N over the range $0{\cdot}01 < \sigma < 100$. It remains to be seen whether the enhancement of N at low σ occurs for three-dimensional convection. This is to be the subject of a subsequent investigation.

5.5. *The Rayleigh number*

The variation of N and $\mathscr{M}$ with λ is shown in figures 4 (*c*) and (*d*). As λ increases a boundary layer in the entropy gradient develops. The horizontal average of the entropy as a function of x_2 is shown in figure 5 for a number of values of λ. Each

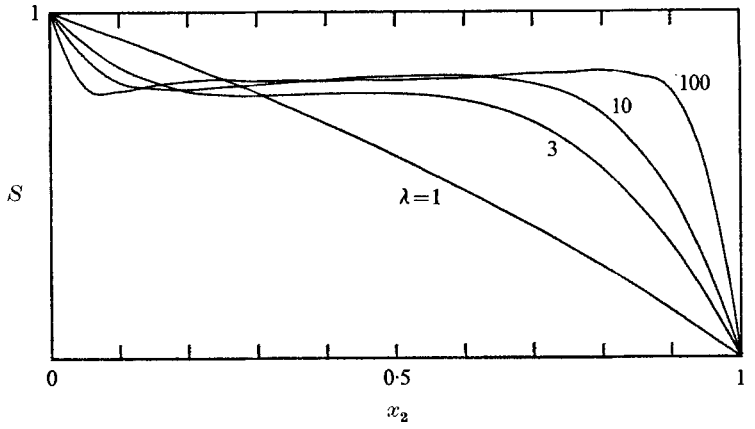

FIGURE 5. Mean normalized entropy as a function of depth for a number of values of the relative Rayleigh number. Grid size = 21 × 21.

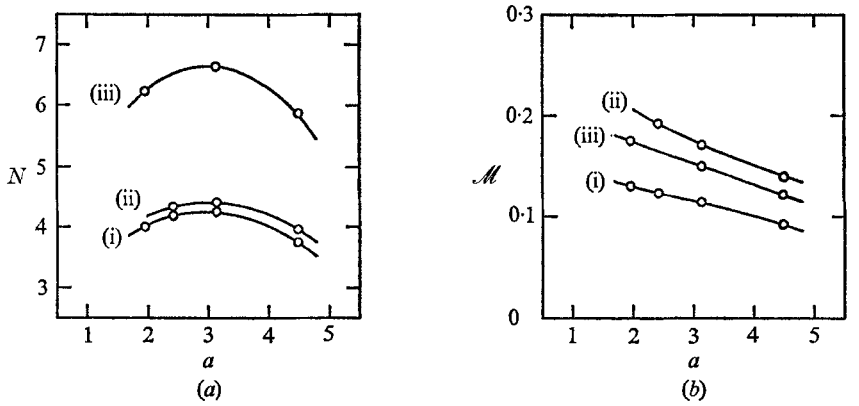

FIGURE 6. Nusselt number and maximum Mach number as functions of wavenumber for the cases (i) $R = 4211{\cdot}9$, $Z = 1$, (ii) $R = 4211{\cdot}9$, $Z = 2$, (iii) $R = 12\,635$, $Z = 1$. 21 grid points in the vertical direction.

curve is normalized to have the same maximum and minimum value. For large λ, the entropy is nearly constant except near the boundaries. The increasing sharpness of the boundary layers sets an upper limit on the value of λ that can be used with a particular finite-difference grid, if the boundary layer is to be adequately resolved.

5.6. *The wavenumber*

Our choice of constant λ is not appropriate if we are investigating the effects of changing the wavenumber. In a medium unbounded in the horizontal, the Rayleigh number can be prescribed but the relative Rayleigh number cannot since R_c is a function of a and the fluid is free to choose its own value for a. The effect on N and $\mathscr{M}$ of varying a while holding R constant is shown in figures 6 (*a*) and (*b*) for three pairs of values of R and Z. The variation of a was effected by changing the aspect ratio A of the cell. If we denote by a_m the wavenumber which maximizes the heat flux, we see that a_m is insensitive to R and Z. In the three

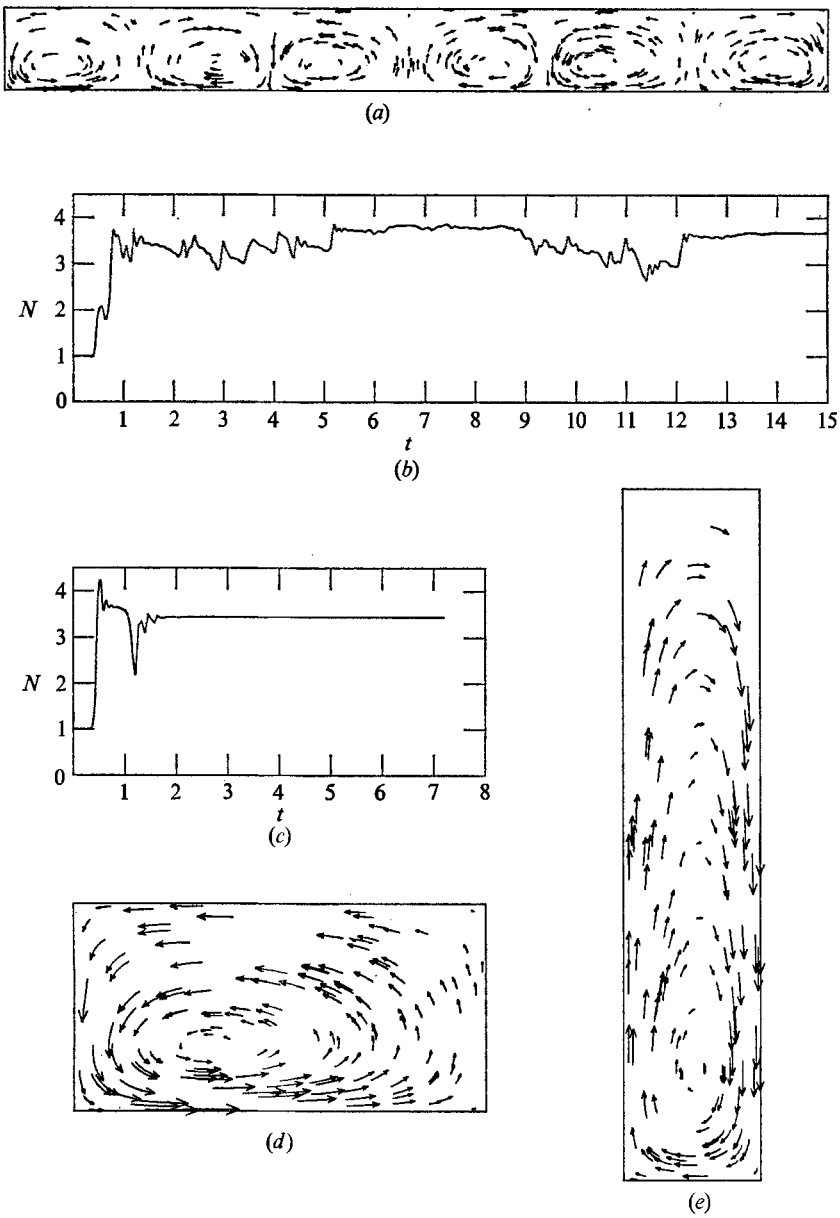

FIGURE 7. Solutions with different aspect ratios. (*a*) Velocity field for $A = 10$, grid size $= 61 \times 7$. (*b*) Time variation of Nusselt number for $A = 10$. (*c*) Time variation of Nusselt number for $A = 2$, grid size $= 13 \times 7$. (*d*) Velocity field for $A = 2$. (*e*) Velocity field for $A = 0{\cdot}2$, $Z = 10$, grid size $= 9 \times 41$.

cases shown, a_m is larger than the critical wavenumber for the linear stability problem. The problem of determining the preferred wavenumber in a horizontally unbounded layer is straightforward in principle. We increase the aspect ratio of the cell and observe the limiting value of a. Increasing A requires an increase in the number of grid points employed in the finite-difference scheme.

Figure 7 (*a*) shows the velocity field for the case $A = 10$. The time for the system to come to equilibrium increases as A is increased. The variation of N with time is shown in figure 7 (*b*). For the case $A = 2$, shown in figures 7 (*c*) and (*d*), the value of N approaches its equilibrium value more rapidly. The initial velocity field for the case $A = 10$ was given by (5.7) and (5.8) with $N_x = 20$ and $N_y = 2$. This ensured that some energy was present in all the modes that are likely to be important in the problem. The time scale for the irregular fluctuations in N was equal to the convective turnover time scale, or about ten times the sound travel time between the upper and lower surfaces. The fluctuations were interpreted as being caused by the interaction of convective rolls with one another. In the case $A = 10$ seven consecutive rolls formed at $t = 6$. The solution remained almost steady until $t = 9$, when the velocity field readjusted to produce six rolls. The integration in time was extended to $t = 20$ but no further changes in the velocity field occurred. The seven-roll solution has a wavenumber $a = 2{\cdot}2$, which is close to a_c, but smaller than a_m. The six-roll solution has $a = 1{\cdot}88$, a value smaller than either a_c or a_m. The value of N is smaller for the six-roll solution than for the seven roll solution. In this case the preferred mode is not the one which maximizes the heat flux.

We have also constructed solutions with $A = 0{\cdot}2$ to see if the flow breaks up into a series of rolls in the vertical. No solutions of this form were found. The case $Z = 10$, where the vertical stratification is such that the pressure varies by a factor of 300 between the upper and lower surfaces, is shown in figure 7 (*e*).

6. Summary and conclusions

In the parameter range and for the initial conditions considered, unique steady solutions were found. The length of time required to reach a steady state increased as the aspect ratio A of the cell increased. For larger values of A than those considered, it is possible that no stable steady state exists.

The failure to find solutions with a vertical distribution of rolls has some significance for astrophysical convection theory. It has generally been assumed that the mixing length should be taken as the smaller of the pressure (or density) scale height and the physical dimension of the system. In our case we find that coherent motions can extend over several scale heights. It remains to be seen whether this holds true for the three-dimensional convection at the large values of R encountered in stellar convection zones.

The present paper illustrates the feasibility of using finite-difference methods to obtain numerical solutions of the full equations for compressible convection. The inclusion of variable conductivity, viscosity or a more complicated equation of state is straightforward. The difference scheme shows remarkable stability and has been extended to three dimensions, although the amount of computing time required will probably rule out a survey of the type presented here. The use of a finite-difference method precludes the possibility of treating the motions with the greatly differing length scales expected at high values of R. It would not be difficult to introduce an eddy diffusion coefficient into the numerical scheme to handle, at least in a crude way, the motions of sub-grid scale.

The solutions presented here provide a useful check on other more approximate treatments of convection. In a future paper, we shall give the results of comparing truncated series solutions of the anelastic equations with the solutions of the full equations.

This work was supported in part by the National Science Foundation under NSF GP32336X. Most of the computation was performed at the University of Cambridge Computer Laboratory. The program development and testing took place at the Goddard Institute for Space Studies, New York City, and I am grateful to Dr R. Jastrow for making this facility available.

REFERENCES

GOUGH, D. O. 1969 *J. Atmos. Sci.* **26**, 448.

LATOUR, J. 1972 Ph.D. thesis, University of Nice.

LATOUR, J., SPIEGEL, E. A., TOOMRE, J. & ZAHN, J.-P. 1974 In preparation.

MOORE, D. R. & WEISS, N. O. 1973 *J. Fluid Mech.* **58**, 289.

OGURA, Y. & PHILLIPS, N. A. 1962 *J. Atmos. Sci.* **19**, 173.

RICHTMYER, R. D. & MORTON, K. W. 1967 *Difference Methods for Initial Value Problems.* Interscience.

SPIEGEL, E. A. 1965 *Astrophys. J.* **141**, 1068.

SPIEGEL, E. A. 1971 *Ann. Rev. Astron. Astrophys.* **9**, 323.

SPIEGEL, E. A. 1972 *Ann. Rev. Astron. Astrophys.* **10**, 261.

SPIEGEL, E. A. & VERONIS, G. 1960 *Astrophys. J.* **131**, 442.

VICKERS, G. T. 1971 *Astrophys. J.* **163**, 363.